Wetting Properties of the CO_2–Water–Calcite System via Molecular Simulations: Shape and Size Effects

A. Silvestri,*,† E. Ataman,‡ A. Budi,¶ S. L. S. Stipp,§ J. D. Gale,† and P. Raiteri†

†*Curtin Institute for Computation, The Institute for Geoscience Research (TIGeR), School of Molecular and Life Sciences, Curtin University, PO Box U1987, Perth, WA 6845, Australia*

‡*Nano-Science Center, Department of Chemistry, University of Copenhagen, Universitetsparken 5, København Ø DK-2100, Denmark*

¶*Institute for Frontier Materials, Deakin University, Geelong, VIC 3216, Australia*

§*Department of Physics, Technical University of Denmark, Fysikvej, DK-2800, Kongens Lyngby, Denmark.*

E-mail: alessandro.silvestri@curtin.edu.au

Abstract

Assessment of the risks and environmental impacts of carbon geosequestration requires knowledge about the wetting behavior of mineral surfaces in the presence of CO_2 and the pore fluids. In this context, the interfacial tension (IFT) between CO_2 and the aqueous fluid and the contact angle, θ, with the pore mineral surfaces are the two key parameters that control the capillary pressure in the pores of the candidate host rock. Knowledge of these two parameters and their dependence on the local conditions of pressure, temperature and salinity is essential for the correct prediction of structural and residual trapping. We have performed classical molecular dynamics simulations to predict the CO_2–water IFT and the CO_2–water–calcite contact angle. The IFT results are consistent with previous simulations, where simple point charge water models have been shown to underestimate the water surface tension, thus affecting the simulated IFT values. When combined with the EPM2 CO_2 model, the SPC/Fw water model indeed underestimates the IFT in the low pressure region at all temperatures studied. On the other hand, at high pressure and low temperature, the IFT is overestimated by $\sim$5 mN/m. Literature data regarding the water contact angle on calcite are contradictory. Using our new set of force field parameters, we performed NVT simulations at 323 K and 20 MPa to calculate the contact angle of a water droplet on the calcite {10.4} surface in a CO_2 atmosphere. We performed simulations for both spherical and cylindrical droplet configurations for different initial radii, to study the size dependence of the water contact angle on calcite in the presence of CO_2. Our results suggest that the contact angle of a cylindrical water droplet on calcite {10.4}, in the presence of CO_2, is independent of droplet size, for droplets with a radius of 50 Å or more. On the contrary, spherical droplets make a contact angle that is strongly influenced by their size. At the largest size explored in this study, both spherical and cylindrical droplets converge to the same contact angle, 38°, indicating that calcite is strongly wetted by water.

Introduction

Burning fossil fuels had led to increased atmospheric CO_2 and is one of the main drivers for global climate change and ocean acidification.[1] Carbon geosequestration in deep saline formations and depleted oil and gas reservoirs represents a promising option for reducing the amount of CO_2 in the atmosphere[2] but other porous formations can also be used, such as basalt, in the successful CarbFix method.[3] Successful carbon sequestration requires that CO_2 is trapped in a geological unit with minimum risk of leakage, while at the same time, environmental impact is minimised. Once injected into a geological formation, the fate of CO_2 depends on the interfacial interactions with the pore mineral surfaces and the solution that occupies the pores. The dominant parameters include: interfacial tension (IFT), wettability, capillarity and mass transfer.[4,5]

In the initial stages of CO_2 sequestration in geologic media, structural and residual trapping provide the highest trapping contribution.[2,4,5] In most rock formations, the pore fluids are saline and because the injected supercritical CO_2 is typically less dense, it migrates upward by buoyancy. Structural trapping refers to retention by a low porosity cap rock seal that prevents CO_2 from migrating further upward and diffusing into the atmosphere. Access to the cap rock pore network is controlled by the capillary entry pressure, P_c, which is the difference between the pressure of two immiscible fluid phases – in this case CO_2 and water – in a tight pore of radius, R. P_c is related to the IFT between the two phases and the water contact angle through the Young–Laplace equation;

$$P_{\mathrm{c}} = P_{\mathrm{W}} - P_{\mathrm{C}} = \frac{2\gamma_{\mathrm{WC}} \cos\theta_{\infty}}{R}, \qquad (1)$$

where γ_{WC} represents the IFT between the aqueous phase and the CO_2 rich phase, θ_{∞} represents the contact angle formed by the macroscopic bulk phases on the mineral surface and R, the radius of the largest connected pore aperture in the cap rock. For trapping to be effective, the capillary pressure must be higher than the buoyant force.

Residual trapping takes place when small CO_2 bubbles are left behind in the pores of the formation. Capillary pressure works on the interface between CO_2 bubbles, the pore solution and the pore surfaces, to prevent the residual CO_2 from migrating upward. The wetting behavior of the solid surfaces controls the ratio of mobile to residually trapped CO_2. The equilibrium contact angle of a non-reactive liquid on a smooth, homogeneous, rigid, and insoluble solid balances the interfacial tensions between the macroscopic bulk phases, through Young's equation;[6]

$$\cos\theta_{\infty} = \frac{\gamma_{\mathrm{MC}} - \gamma_{\mathrm{MW}}}{\gamma_{\mathrm{WC}}}, \qquad (2)$$

where γ_{MC} and γ_{MW} represent the mineral–CO_2 and mineral–water interfacial tensions. Low contact angles indicate good wetting of the solid by the liquid, whereas large angles indicate poor wetting. It has been shown that CO_2-wetting has a negative impact on residual trapping, with water wet surfaces trapping approximately 240% more CO_2 over a period of 10 years than CO_2-wet minerals.[7]

To assess the extent of structural and residual trapping, the interfacial properties of the CO_2–water–mineral system need to be better understood.[4,7] Experimental determination of the CO_2–water (or saline solution) IFT requires accurate phase density measurements, which are difficult to make. Published IFT experimental data vary widely and only few studies have reported high-quality data over the full range of relevant P and T conditions.[8] Despite the variability and uncertainties in published data, especially close to the CO_2 critical point and at high pressure, the experimental consensus is that IFT: i) decreases sharply with increasing pressure in the CO_2 subcritical region and reaches a plateau in the supercritical region,[9] ii) decreases with increasing temperature at low and high pressures but has a more complex temperature dependence around the CO_2 critical point[10] and iii) increases linearly with salt concentration.[11] Contact angle measurements have been performed on a wide variety of mineral substrates, typically quartz and mica, and these are assumed to be representa-

tive of silicate formations. Only a few studies have reported the contact angle on a calcite substrate that is representative of carbonate formations.[12–18] The experimental results are consistent, in that the calcite system is strongly water-wet ($0°<\theta<75°$), but there is significant scatter in the reported contact angles, ranging from $\sim 2°$ to $60°$.[7,19] This is not surprising because organic material and adsorbed ions can dramatically change the wettability of mineral surfaces[20,21] and calcite is know to be very attractive to organic material even in very dilute solutions.[22] AFM data and simulation results suggest this to result from adsorption on the ordered water layers that are adsorbed on the calcite surface, rather than direct binding.[23,24] Furthermore, it is known that the surface properties of calcite depend heavily on the history of its exposure.[22] CO_2 speciation changes the chemistry of the water droplet and calcite reacts with the acidified solution leading to mineral dissolution, thus changing the local surface morphology.[12,16,17]

Classical molecular dynamics (MD) simulation has proven to be a powerful tool for investigating wetting phenomena in CO_2–water–mineral systems. MD has been used to predict the interfacial tension between CO_2 and water (or saline solution)[8,25–36] and the contact angle of CO_2–water–mineral surfaces[27,30,32,35–42] as a function of pressure, temperature and salinity. However, while the accuracy of the predicted interfacial tension only depends on the ability of the force fields to reproduce the interfacial energies, the contact angle determination presents a few more challenges. Macroscopic fluid droplets that are measured in experiments have dimensions on the order of mm and even if system sizes accessible to MD simulations are now close to the smallest experiments, the amount of simulation that is required to conduct a systematic study limits us to the nanometer scale. A macroscopic droplet has bulk liquid properties and a circular contact line large enough that one can ignore the curvature effects on the contact angle. On the other hand, surface forces between the solid substrate and liquid modify the shape of the liquid at the nanometer scale and the contact angle θ of a spherical nanodroplet is affected by the curvature of the three-phase contact line. The size dependence of the contact angle has been characterized both in experiments[43–45] and in molecular simulations[46–50] and it is often rationalized by introducing the concept of a contact line tension,[51,52] the excess free energy per unit length of the three-phase contact line, that results from an imbalance of forces between molecules existing in and around the zone at which the three phases meet.[53] This effect is accounted for by adding a correction term to Equation 2;

$$\cos\theta = \cos\theta_\infty - \frac{\kappa}{\gamma_{\mathrm{WC}}}\frac{1}{r}, \qquad (3)$$

where $\cos\theta_\infty$ is given by Equation 2, κ represents the line tension and $1/r$, the curvature of the three-phase contact line. All the deviations and shortcomings of Young's Equation are collected in the value of κ. The line tension effect is weak and its experimental determination is challenging because it requires ideal surfaces without heterogeneity. In addition, its influence on contact angle is considered significant only for droplets with a diameter ranging from one to a few hundred nanometers and it is difficult to produce and control such droplets in experiments. As a result, there is no consensus on either the magnitude of κ, which is in the range from 10^{-5} to 10^{-11} N, or its sign, which can be either positive or negative, depending on the nature of the phases around the contact line.[53,54] The majority of simulation studies have solved this problem by adopting a cylindrical droplet configuration, for which the three-phase contact line is straight, thus eliminating the contribution of line tension caused by curvature in Young's equation. However, Scocchi *et al.*[49] found that the contact angle of a SPC/Fw water cylindrical filament on graphite also depends on the droplet radius, demonstrating that a cylindrical configuration is also affected by size effects.

Atomistic simulations are barely beginning to be applied to predict contact angles on mineral surfaces[55] and all the above reported studies, apart from the work of Tenney and Cygan[39] on kaolinite, focused on silica surfaces. One of the main reasons why calcite has been ignored in

modelling studies so far is most likely the lack of reliable force field parameters for its interaction with CO_2. The purpose of this study was to use our new set of force field parameters[24] to predict the contact angles in the CO_2–water IFT and CO_2–water–calcite systems. We have conducted a comparative investigation by simulating spherical droplets and cylindrical filaments of equivalent size to show the results of using different configurations and to verify at which length scales, size effects on the contact angle become negligible.

Methods

Molecular models

A few simplifications were necessary to model the CO_2–water–carbonate mineral system. First, real injection site conditions are far too complex to allow inclusion of all of the details for modelling so we simplified to a pure calcite surface of only crystalline $CaCO_3$, pure CO_2 in either gas or supercritical phase and pure water. Second, including pH effects explicitly in our simulations is not straightforward because it would require a large number of water molecules to achieve the appropriate hydrogen ion concentrations. Gale *et al.*[56] proposed a reactive force field that allows modelling of speciation in the aqueous calcium carbonate system but the predicted thermodynamics might not be accurate enough to reproduce pH observed in experiments. In addition, at the relatively high pressure conditions for the simulations, molecular CO_2 is the dominant species. For these reasons, we decided not to include any of the products of CO_2 speciation in aqueous solution in our simulations of the CO_2–water interface. The absence of any chemistry in our model means that we cannot observe any change in the calcite surface morphology that would result from dissolution.

All of the simulations were performed using the LAMMPS package.[57] For calcite, we used the thermodynamically consistent force field of Raiteri *et al.*[58] Water was modelled with the SPC/Fw force field,[59] which incorporates harmonic bond stretching and angle bending potentials into the SPC model. This water model has been shown to be transferable to high temperatures[58] and supercritical conditions[60] and it gives good predictions of the water dielectric constant and surface tension.[61] For CO_2, we used the elementary physical model (EPM2)[62] with the bond stretching and angle bending terms from Cygan *et al.*[63] The incorporation of flexible bonds in water and CO_2 potential models does not change the computed phase boundaries appreciably[55] and allows for better predictions of water surface tension.[64] The water–CO_2 cross terms are obtained by applying the Lorentz–Berthelot mixing rules:

$$\epsilon_{ij} = \sqrt{\epsilon_i \epsilon_j} \tag{4}$$

and

$$\sigma_{ij} = \frac{\sigma_i + \sigma_j}{2}, \tag{5}$$

where ϵ and σ represent the Lennard–Jones parameters. The interactions between CO_2 and calcite were described by our new set of force field parameters.[24] For van der Waals CO_2–CO_2, water–water and CO_2–water interactions, we used a cutoff distance of 10 Å, whereas for the dispersion interactions of calcite with both CO_2 and water, we used the tapering function of Mei *et al.*;[65]

$$x = \frac{r - r_t}{r_c - r_t} \tag{6}$$

and

$$f(x) = \begin{cases} 1 & \text{if } r < r_t \\ (1 + 3x + 6x^2)(1 - x)^3 & \text{if } r_t \leq r \leq r_c \\ 0 & \text{if } r > r_c \end{cases}, \tag{7}$$

where we used 6 Å for r_t and 9 Å for r_c. Increasing the LJ cutoff leads to no significant improvement in the results (Figure S1, Supporting Information). A cutoff of 10 Å was used for the real space contribution to the electrostatic interaction and the reciprocal space electrostatics were calculated using the PPPM algorithm[66] with an accuracy of 10^{-5}.

Table 1: Initial droplet radius, approximate total number of atoms and water molecules for hemispherical droplets and hemicylindrical filaments. Half of the distance between the contact lines is used as the radius for the cylindrical droplet.

Hemisphere			Hemicylinder		
Radius (Å)	Total number of atoms	Water molecules	Radius (Å)	Total number of atoms	Water molecules
25	220,000	1,100	25	70,500	1,550
37	275,000	3,450	37	74,000	3,450
50	286,000	8,700	50	147,000	6,300
63	845,000	17,400	63	154,000	10,000
75	860,000	29,400	75	161,000	14,300

Simulation method

For all simulations, the cell volume was controlled with the Parrinello–Rahman algorithm,[67] with a relaxation time of 1 ps and the cell angles were kept at 90°. Temperature was controlled using a Nosé–Hoover chain of thermostats[68] of length 5 with a relaxation time of 0.1 ps. Periodic boundary conditions were applied in all directions for all simulations. The equations of motion were integrated with a time step of 1 fs. All systems were energy minimized before starting the molecular dynamics simulations. Atomic configurations were stored every 1,000 steps (1 ps) for trajectory analysis.

For the simulation of the CO_2–water interface, we selected P and T conditions covering the range relevant for carbon geosequestration:[10] For temperatures of 308, 323 and 383 K, we ran simulations for pressures in the range 1–50 MPa. We used cells with dimensions of 49.32 Å × 48.55 Å in x and y and variable starting dimensions along z, the direction normal to the interface. The number of water molecules was chosen to be 3,000, while the number of CO_2 molecules was 2,000 (850–1,000 for systems at p =1 MPa). With these dimensions, the system achieves bulk phase properties in both fluid phases and the predicted IFT is not influenced by the size of the simulation cell.[8] We performed 30 ns long $NP_{zz}T$ simulations at the chosen pressure and temperature. After equilibration, two thermodynamically stable phases, separated by an interface normal to the z axis, were formed. The interfacial tension between CO_2 and water was calculated from the principal components of the MD simulation cell stress tensor,[69] using the relation:

$$\gamma_{WC} = \frac{1}{2} L_z \left[P_{zz} - \frac{1}{2}(P_{xx} + P_{yy}) \right] \qquad (8)$$

where L_z represents the interface-normal simulation cell length, P_{zz} represents the interface-normal pressure component and P_{xx} and P_{yy}, the interface-parallel pressure components of the cell stress tensor. The systems reach thermodynamic equilibrium within 2 ns. The first 5 ns of trajectory was excluded from the analysis and the remaining 25 ns was divided in 5 segments of 5 ns each. The IFT was calculated at each step and averaged values were determined for each segment. The reported IFTs and their statistical errors were obtained by averaging the results from the five trajectory segments.

Once the force fields had been demonstrated to provide reliable results for the CO_2–water interfacial tension, we built further models for contact angle simulations. We performed a series of MD simulations using water droplets of different sizes. We used spherical droplets and cylindrical filaments of equivalent radii that, apart from the different number of particles, were studied at otherwise identical conditions. The simulated cells are summarized in Table 1. For the largest system, adopting a cylindrical configuration allowed the number of atoms to be reduced by a factor of 5. Figure 1 shows the hemispherical (a) and hemicylindrical (b) configurations for the largest system studied in

this work. The calcite slab was 12 layers thick and the length of the slab was varied according to the droplet shape and size. Hemispherical and hemicylindrical droplets were extracted from 3 different average density frames selected from an NPT equilibrated CO_2–water cell at 20 MPa and 323 K. This was done to generate different starting configurations for each system and to collect statistics. Droplets with different starting radii were placed ∼2 Å above the calcite surface at the beginning of the simulations. The remaining cell volume was filled with a CO_2-rich phase, again extracted from the above mentioned frames. A cavity was created in the CO_2-rich phase close to the calcite surface to make space for the droplet. For spherical droplets, we used planes that ranged approximately from 200×200 to 400×300 Å^2. For cylindrical droplets, we used rectangular planes with a thickness of ∼48.55 Å and length ranging from 200 to 400 Å, depending on the size of the hemicylindrical droplet. The length of the simulation box in the z direction was chosen to be large enough to prevent any interaction between periodic images for any of the simulated models. After energy minimization, we performed 30 ns long NVT simulations for all systems.

The contact angle was calculated from the water axial-radial density profiles, by averaging 20,000 postequilibrium MD simulation snapshots, distributed over a period of 20 ns. Simulation cells were divided into bins of equal volume for analysis of the density distribution. The cylinder axis runs parallel to the y direction, therefore the xz-plane is considered for the hemicylindrical droplets while both xz- and yz-planes are used for the hemispherical droplets. From the 2D density profile, we extracted the water density along the axis of symmetry of the droplet. Following the procedure of de Ruijter *et al.*,[70] we located the CO_2–water interface by fitting the profile with the hyperbolic tangent function:

$$\rho(z) = \rho_0 \left[1 - \tanh\left(\frac{z - z_0}{d}\right)\right], \qquad (9)$$

where z_0 represents the point where the water density, ρ_0, is halfway between its liquid bulk

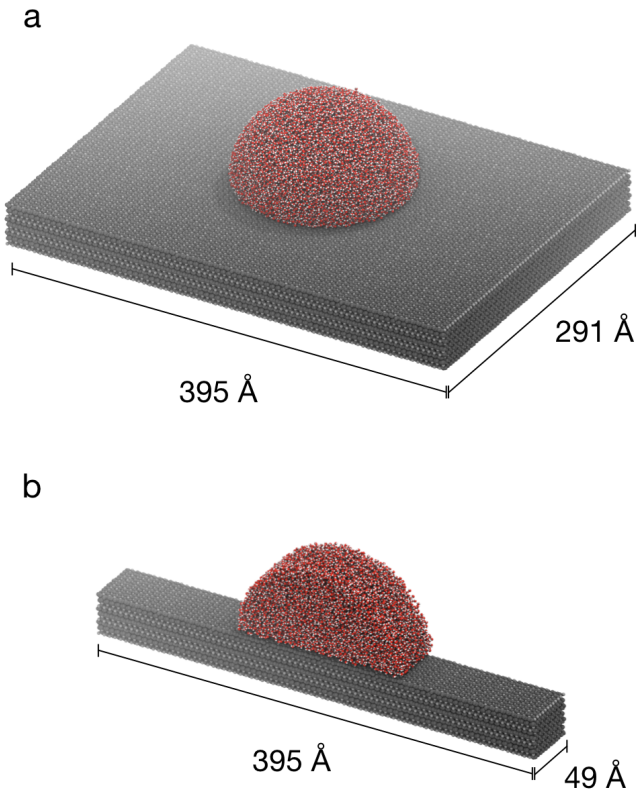

Figure 1: Hemispherical (a) and hemicylindrical (b) droplets for the largest system studied. Oxygen atoms are represented in red, hydrogen in white, carbonate ions in dark grey and calcium ions in light gray. CO_2 molecules are not included in the representation for clarity.

value and its value in the CO_2 phase and d represents the width of the CO_2–water interface. Applying the sigmoidal fit, we can uniquely determine the CO_2–water interface (Figure 2). Isodensity contours (in g/cm^3) at $\rho = \rho_0 - 0.1$, $\rho = \rho_0$ and $\rho = \rho_0 + 0.1$ (Figure 3) were then plotted. Away from the mineral surface, the droplet density contours have the shape of a spherical cap but near the surface, they reflect water layering adjacent to the surface and their shape departs from a circle. To avoid the influence of density fluctuations at the water–calcite interface, the region that extends for about 10 Å from the calcite surface into the droplet was disregarded. A circular profile was fit to the droplet contours and the droplet base radius, b, and height, h, were calculated. The contact angle was finally determined via:

$$\theta = \arcsin \frac{2hb}{h^2 + b^2}, \qquad (10)$$

For the base of the droplet, we used the position of the third layer of water out from the calcite interface. The resulting contact angles differed only by a few tenths of a degree and we therefore report the value for the isodensity line at $\rho = \rho_0$ for all of the systems studied.

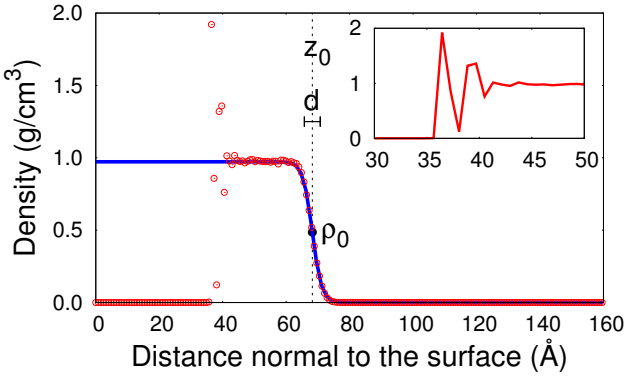

Figure 2: Density profile along the axis passing through the center of the droplet and normal to the surface as a function of the distance normal to the surface. The red circles represent the data and the solid blue line is the fit with the hyperbolic tangent function of Equation 9. The inset shows the oscillating density profile near the calcite surface, where the axis labels and units are as in the main figure.

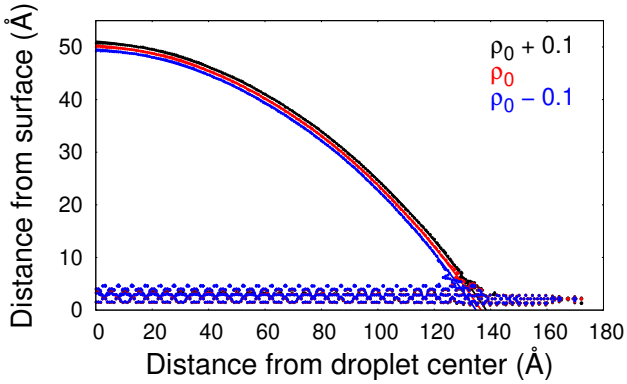

Figure 3: Isodensity contours (points) fitted by circles (straight lines) for three layers of water around the CO_2–water interface. Density is expressed as g/cm^3.

Results and discussion

Interfacial tension

A survey of the literature suggests that molecular dynamics simulations give inconsistent predictions of water surface tension and that the discrepancies in the results can be ascribed to the differences among the water models, such as the inclusion of flexibility in the O–H bond, and simulation parameters, e.g. simulation time, LJ cutoff and the treatment of electrostatic interactions.[61] The most commonly used fixed charge water models, such as the SPC/E model, underestimate water surface tension by up to 10 mN/m and this inaccuracy affects the values of interfacial tension at low CO_2 pressure.[8] López-Lemus *et al.*[64] found that the incorporation of flexibility to the intramolecular degrees of freedom of the SPC/E model led to a higher value for the water surface tension, closer to the experimental data. Yuet and Blankschtein[61] compared the results of various flexible water models and observed a difference of approximately 8% in the predicted water surface tension when the LJ cutoff was changed from 10 to 24.5 Å, with the longer cutoff giving better agreement with the experimental results. In their study, the SPC/Fw model gave a water surface tension that was about 11% lower than that found in experiments and the best prediction of the water dielectric constant, which is an important factor when considering electrolytes in solution. We explored the effect of changing the LJ cutoff on predicted CO_2–water IFTs at 1 MPa and 323 K. The results are summarized in Figure S1 of the Supporting Information. Increasing the LJ cutoff from 10 to 24 Å did not improve the results dramatically, while the longer cutoff increased the computational cost by more than a factor of two. For this reason, simulations were run using an LJ cutoff of 10 Å.

Figure 4 show the predicted CO_2–water interfacial tension along with the experimental data of Chiquet *et al.*[10] and Kvamme *et al.*[26] and the molecular dynamics predictions of Nielsen *et al.*,[8] Liu *et al.*,[29] Javanbakht *et al.*[32] and Liang *et al.*[36] In general, our results agree well with previous simulations and give similar er-

rors when compared to experimental data. As expected, the inability of the force field to reproduce the water surface tension reflects in the IFT results at low pressure at all temperatures. Still, the EPM2-SPC/Fw combination offers better quantitative agreement with experiment when compared to the TraPPE-TIP4P2005 combination and a similar performance to the SPC/E force field. At 323 K, our simulations predict the IFT plateau to be at lower pressure and this could be explained by the fact that using a short LJ cutoff results in a slight reduction in the critical temperature of CO_2 predicted by the EPM2 model.[27] It is interesting, that previous results for 1 M NaCl solutions[29] closely follow the experimental data for pure water, even if the IFT increases linearly with salt concentration.[11] Our results at 383 K are in good agreement with previous simulations where the SPC/E water model was used. Nielsen *et al.*[8] suggested that the results of simulations using the SPC/E water model should be renormalized to have them correspond with the measured water surface tension. To this end, the difference between the experimental and simulated surface tension of pure water at a given temperature can be added to the SPC/E-simulated CO_2–water IFTs, to reflect the results obtained from a water model that reproduces the experimental water surface tension. However, because this is a renormalization additive correction rather than a scaling factor, this would result in larger deviations from experiment at high pressure. Indeed, at 308 and 323 K, the predicted IFTs are about 5 mN/m higher than the experimental data. Iglauer *et al.*[27] explained that the accuracy of the water force field is essential for quantitative agreement with experiment at low to intermediate pressures and plays a less important role at high pressures. They explained the overprediction of IFTs by suggesting that using Lorentz–Berthelot mixing rules does not consider the non-additive contributions between CO_2 and water, that are important at high pressures (high CO_2 density). According to Li *et al.*,[28] the deviation at high pressures does not result from density deviation but can be due to other simulation parameters such as the system size.

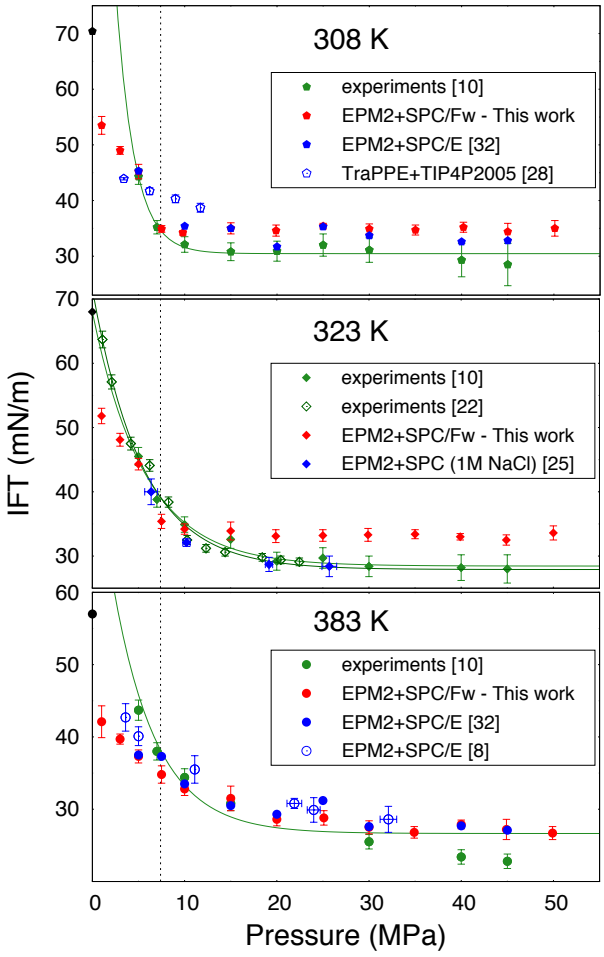

Figure 4: Comparison of predicted IFTs with literature data at 308 K, this study (red pentagons), experimental data from Chiquet *et al.*[10] (green pentagons) and the simulation results of Javanbakht *et al.*[32] (open blue pentagons) and Liang *et al.*[36] (closed blue pentagons), 323 K, this study (red diamonds), experimental data from Chiquet *et al.*[10] (closed green diamonds) and Kvamme *et al.*[26] (open green diamonds) and simulation data from Liu *et al.*[29] (blue diamonds) and 383 K, this study (red circles), experimental data from Chiquet *et al.*[10] (green circles) and simulations results of Nielsen *et al.*[8] (open blue circles) and Liang *et al.*[36] (closed blue circles). The black symbols represent the water surface tension calculated using the IAPWS recommended interpolating equation for the surface tension of ordinary substances[71] at the given temperature. The dashed vertical line represents the CO_2 critical pressure. Experimental data were fit to an exponential function (green line).

Figure 5 shows the predicted CO_2–water interfacial tension as a function of pressure at 308, 323 and 383 K. The qualitative trends of the IFT are correctly predicted:[72] a gradual linear decrease with pressure, a plateau reached at higher P, decreasing IFT with increasing temperature at low and high pressure and a crossover region at intermediate pressure (though more data need to be collected in this region). Temperature influences the pressure at which the plateau is reached as well as the value of IFT at high pressure. We also found that the difference between the IFTs at low and high temperatures decrease with increasing pressure.

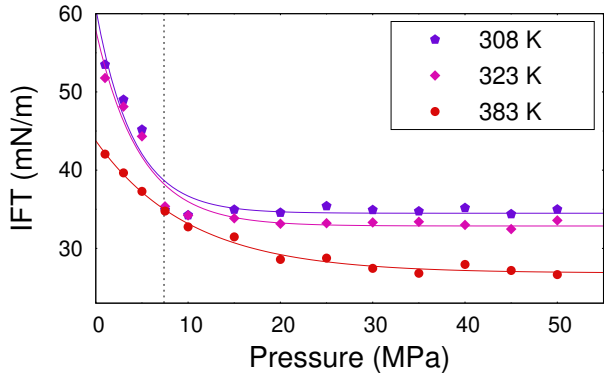

Figure 5: CO_2–water interfacial tension as a function of pressure at 308 K (purple pentagons), 323 K (magenta diamonds) and 383 K (red circles). The vertical dashed black line marks the CO_2 critical pressure (7.39 MPa).

Contact angle

Figure 6 shows the water droplet configuration after it spreads into its equilibrium state. Some of the water molecules manage to escape the water droplet and adsorb on the other side of the calcite slab, after having diffused through the CO_2 layer.

The 2D water profile (Figure 7a) shows that water density is higher at the calcite surface (red). This is consistent with the non-defective calcite basal surface being strongly wetted by water. At least one monolayer of water covers the calcite {10.4} surface and the ordering influence of the mineral structure produces two more structured layers in the droplet. Water ordering by calcite is consistent with experimental data[73,74] and previous MD simulations of water and ethanol on calcite.[75] The 2D CO_2 profile (Figure 7.b) also shows that CO_2 density is high close to the calcite surface away from the droplet. This suggests interaction between the mineral surface and CO_2. We observed a similar but weaker interaction between CO_2 and the {10.4} surface of calcite in our previous simulations[24] where bulk water formed 3 structured layers above the surface, excluding CO_2 from direct interaction with the mineral. In the present study, the calcite slab was not completely hydrated and CO_2 was able to bind more strongly to the surface and the first hydration layer. This leads to structuring of the CO_2 on calcite, giving rise to fluctuations in the density and ordering in the first ∼10 Å.

A typical profile along the axis, passing through the center of the droplet and normal to the surface is presented in Figure 2. Close to the solid, the density oscillates because of the structuring effect of calcite on water. Three layers away from the surface, water reaches its bulk density. Figure 3 shows the density contour lines for three water layers around the CO_2–water interface. As can be seen from the figure, the circular fit represents the contour lines very well, demonstrating that the droplet is shaped as a spherical cap.

In Figure 8, contact angle is plotted against the inverse of the initial radius for both spherical droplets and cylindrical filaments. By comparing spherical and cylindrical droplets of the same initial radius, r_i, we observed that spherical droplets are more sensitive to size variations. For N>6,300 water molecules, the contact angle of a cylindrical droplet was insensitive to size variation. The same condition was reached at N>17,400 water molecules for spherical droplets. The smaller system sizes have smaller contact angles. Spherical and cylindrical configurations converge to ∼38° at the largest droplet size. This opens the possibility of avoiding time consuming spherical droplet simulations for future studies of static wetting properties of water on calcite. However, it should be noted that cylindrical filaments are also size-dependent for small numbers of wa-

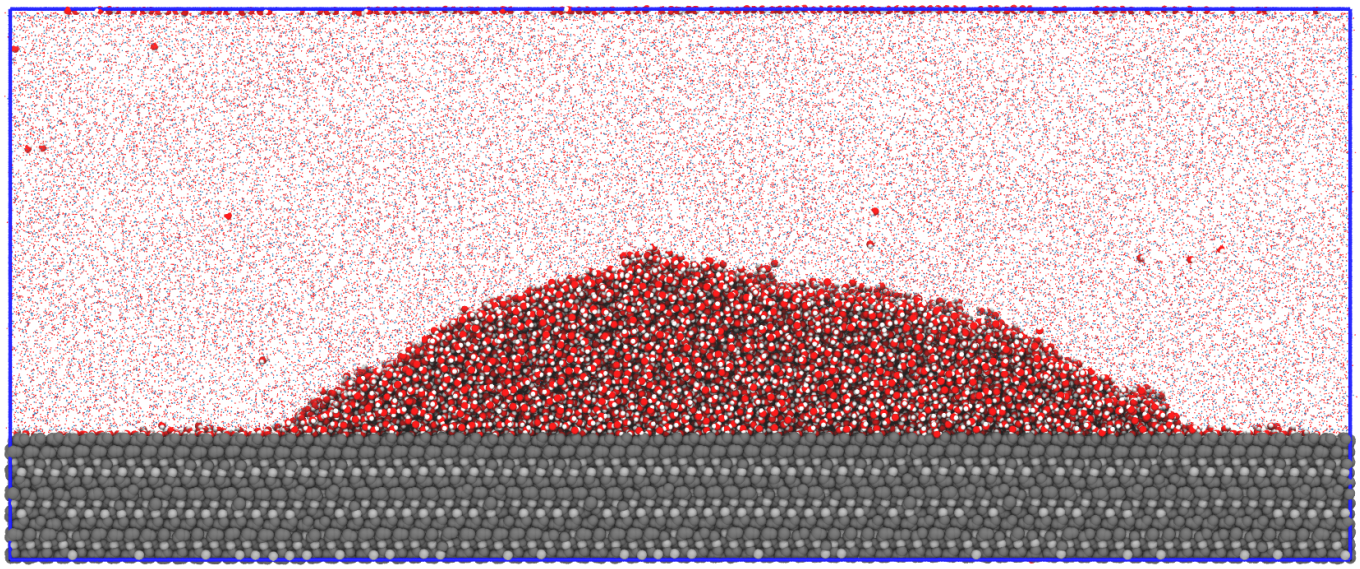

Figure 6: Water droplet configuration on calcite {10.4}, after 30 ns of NVT simulation at 323 K for the largest cylindrical droplet. The color code is the same as in Figure 1 but now, CO_2 molecules are included and represented as dots (blue for carbon and red for oxygen).

ter molecules (N<3,500). This effect cannot be explained in terms of line tension, because in cylindrical filaments the three-phase contact line has zero curvature. According to Scocchi *et al.*,[49] the decreasing contact angle with decreasing droplet size originates from the fact that molecules near the contact line experience reduced cohesive forces because of the higher curvature of the liquid dividing surface and this results in an increase in the adhesive component of the total force acting on them. This effect goes in the opposite direction of a line tension effect and it dominates even in the case of spherical droplets, where a positive line tension would act by increasing the contact angle with decreasing droplet size. In general, as the droplet or filament grows smaller, the number of molecules that belong to the most superficial layer of the droplet increases relative to those in the bulk and this results in the reduction of the cohesive forces acting on the molecules near the contact line and in the decrease of the contact angle. The contact angle for the largest droplets in this study was about 38°, which closely follows the experimental results of Espinoza *et al.*[12] and Bikkina *et al.*,[13] though more simulations are needed to study the effects of pressure, temperature and salinity on the contact angle.

Summary and Conclusions

When combined with the EPM2 CO_2 model, the SPC/Fw water model underestimates the water surface tension at low pressure and overestimates it at high pressure. This was observed previously in simulations for simple point charge models of water. We performed droplet simulations of the CO_2–water–calcite system at 323 K and 20 MPa, using both spherical and cylindrical droplets. Density profiles showed that calcite structures both water and CO_2. Contact angle is affected by droplet size, but spherical droplets are more sensitive. Contact angle for large droplets converges to ∼38°, indicating strongly water wetting behavior for calcite. Spherical configurations require expensive simulations because of the large number of particles whereas simulations with cylindrical are faster because of the ability to take advantage of periodic boundary conditions and a shorter box dimension in the direction parallel to the cylinder axes, which reduces the number of atoms. This would allow the use of cylindrical droplets of a converged size for future simu-

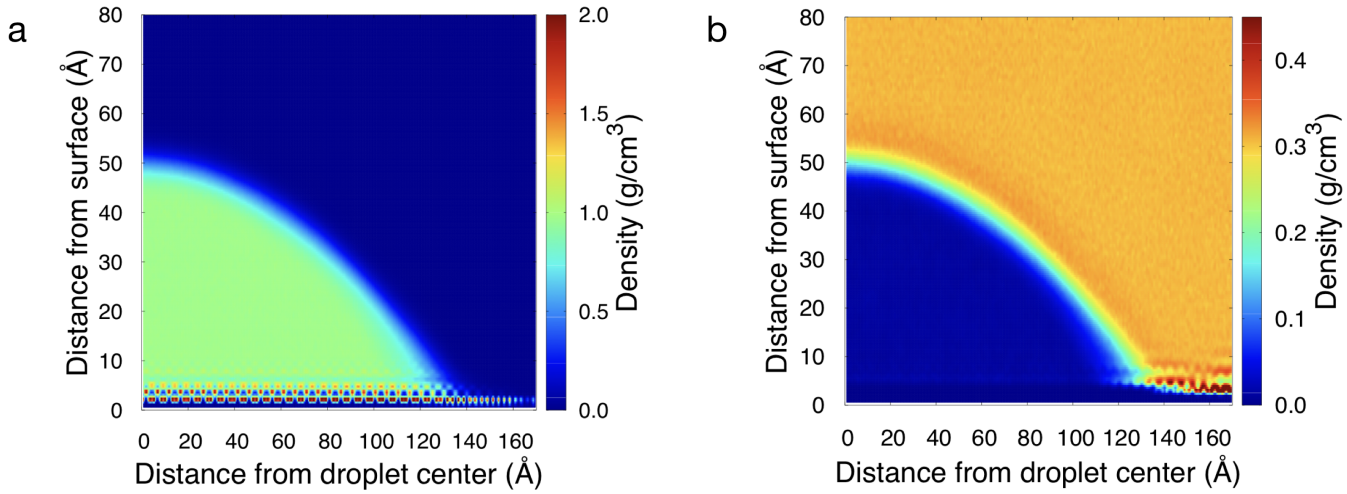

Figure 7: 2D density profile of water (a) and CO_2 (b) corresponding to the largest cylindrical droplet.

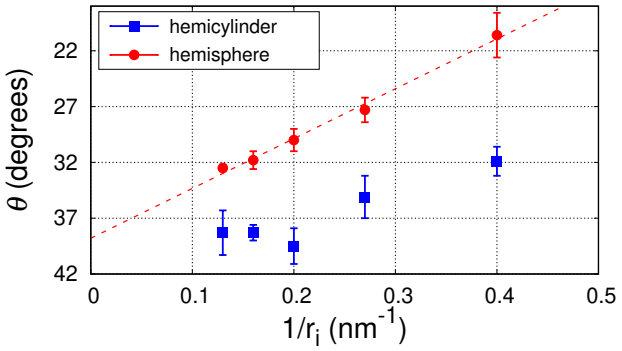

Figure 8: Variation of the water contact angle θ on calcite {1.04} in CO_2 at 323 K and 20 MPa with the inverse of the droplet initial radius r_i.

lations. More simulations are needed to determine the effect of pressure and temperature on contact angle. Finally, a set of force field parameters, for the interaction of CO_2 with dissolved Na^+ and Cl^-, would allow us to simulate the interface between CO_2 and saline solutions and predict the effect of salinity on the system IFT and contact angle.

Acknowledgement This work was partially supported by the Australian Research Council Discovery Programme (FT 130100463, DP160100677, FL0100087). We thank the Australian Government and the Government of Western Australia for providing computational resources through the Pawsey Supercomputing Centre under the National Computational Merit Allocation Scheme. The research visit to Curtin University for A. Silvestri was supported by the NanoGeoScience Laboratories operational budget.

Supporting Information Available

The following files are available free of charge: a plot of the IFT at 323 K and 1 MPa for different LJ cutoffs, a table with computed IFTs and relative errors, a table of computed contact angles for both hemicylindrical and hemispherical configurations, the force field file in LAMMPS format.

References

(1) IPCC 2013, In *Climate Change 2013: The Physical Science Basis. Contribution of Working Group I to the Fifth Assessment Report of the Intergovernmental Panel on Climate Change*; Stocker, T. F., Qin, D., Plattner, G.-K., Tigno, M., Allen, S. K., Boschung, J., Nauels, A., Xia, Y., Bex, V., Midgley, P. M., Eds.; Cambridge University Press, Cambridge, United Kingdom and New York, NY, USA, p 1535.

(2) IPCC, In *IPCC Special Report on Carbon Dioxide Capture and Storage*; Metz, B.,

Davidson, O., de Coninck, H., Loos, M., Meyer, L., Eds.; Cambridge University Press, UK, 2005; p 431.

(3) Gislason, S. R.; Oelkers, E. H. Carbon Storage in Basalt. *Science* **2014**, *344*, 373–374.

(4) DePaolo, D. J.; Cole, D. R. Geochemistry of Geologic Carbon Sequestration: An Overview. *Rev. Mineral. Geochemistry* **2013**, *77*, 1–14.

(5) Bourg, I. C.; Beckingham, L. E.; DePaolo, D. J. The Nanoscale Basis of CO_2 Trapping for Geologic Storage. *Environ. Sci. Technol.* **2015**, *49*, 10265–10284.

(6) Young, T. III. An Essay on the Cohesion of Fluids. *Philosophical Transactions of the Royal Society of London* **1805**, *95*, 84.

(7) Iglauer, S.; Pentland, C. H.; Busch, A. CO_2 Wettability of Seal and Reservoir Rocks and the Implications for Carbon Geo-sequestration. *Water Resour. Res.* **2015**, *51*, 729–774.

(8) Nielsen, L. C.; Bourg, I. C.; Sposito, G. Predicting CO_2–Water Interfacial Tension Under Pressure and Temperature Conditions of Geologic CO_2 Storage. *Geochim. Cosmochim. Acta* **2012**, *81*, 28–38.

(9) Saraji, S.; Goual, L.; Piri, M.; Plancher, H. Wettability of Supercritical Carbon Dioxide/Water/Quartz Systems: Simultaneous Measurement of Contact Angle and Interfacial Tension at Reservoir Conditions. *Langmuir* **2013**, *29*, 6856–6866.

(10) Chiquet, P.; Daridon, J.-L.; Broseta, D.; Thibeau, S. CO_2/Water Interfacial Tensions Under Pressure and Temperature Conditions of CO_2 Geological Storage. *Energy Convers. Manag.* **2007**, *48*, 736–744.

(11) Li, X.; Boek, E.; Maitland, G. C.; Trusler, J. P. M. Interfacial Tension of (Brines + CO_2): (0.864 NaCl + 0.136 KCl) at Temperatures Between (298 and 448) K, Pressures Between (2 and 50) MPa, and Total Molalities of (1 to 5) mol·kg^{-1}. *J. Chem. Eng. Data* **2012**, *57*, 1078–1088.

(12) Espinoza, D. N.; Santamarina, J. C. Water-CO_2-Mineral Systems: Interfacial Tension, Contact Angle, and Diffusion: Implications to CO_2 Geological Storage. *Water Resour. Res.* **2010**, *46*, 1–10.

(13) Bikkina, P. K. Contact Angle Measurements of CO_2-Water-Quartz/Calcite Systems in the Perspective of Carbon Sequestration. *Int. J. Greenh. Gas Control* **2011**, *5*, 1259–1271.

(14) Mills, J. R.; Riazi, M.; Sohrabi, S. M. Wettability of common rock-forming minerals in a CO_2-brine system at reservoir conditions. **2011**, 1–12, 25th International Symposium of the Society of Core Analysts 2011.

(15) Broseta, D.; Tonnet, N.; Shav, V. Are rocks still water-wet in the presence of dense CO_2 or H_2S? *Geofluids* **2012**, *12*, 280–294.

(16) Farokhpoor, R.; Bjørkvik, B. J.; Lindeberg, E.; Torsæter, O. Wettability Behaviour of CO_2 at Storage Conditions. *Int. J. Greenh. Gas Control* **2013**, *12*, 18–25.

(17) Wang, S.; Edwards, I. M.; Clarens, A. F. Wettability Phenomena at the CO_2–Brine–Mineral Interface: Implications for Geologic Carbon Sequestration. *Environ. Sci. Technol.* **2013**, *47*, 234–241.

(18) Arif, M.; Lebedev, M.; Barifcani, A.; Iglauer, S. CO_2 storage in carbonates: Wettability of calcite. *International Journal of Greenhouse Gas Control* **2017**, *62*, 113 – 121.

(19) Arif, M.; Abu-Khamsin, S. A.; Iglauer, S. Wettability of rock/CO_2/brine and rock/oil/CO_2-enriched-brine systems:

Critical parametric analysis and future outlook. *Advances in Colloid and Interface Science* **2019**, *268*, 91 – 113.

(20) Matthiesen, J.; Hassenkam, T.; Bovet, N.; Dalby, K. N.; Stipp, S. L. S. Adsorbed Organic Material and Its Control on Wettability. *Energy & Fuels* **2017**, *31*, 55–64.

(21) Generosi, J.; Ceccato, M.; Andersson, M. P.; Hassenkam, T.; Dobberschütz, S.; Bovet, N.; Stipp, S. L. S. Calcite Wettability in the Presence of Dissolved Mg^{2+} and $SO_4{}^{2-}$. *Energy & Fuels* **2017**, *31*, 1005–1014.

(22) Stipp, S. L.; Hochella, M. F. Structure and Bonding Environments at the Calcite Surface as Observed with X-ray Photoelectron Spectroscopy (XPS) and low energy electron diffraction (LEED). *Geochim. Cosmochim. Acta* **1991**, *55*, 1723–1736.

(23) Nalbach, M.; Raiteri, P.; Klassen, S.; Schäfer, S.; Gale, J. D.; Bechstein, R.; Kühnle, A. Where Is the Most Hydrophobic Region? Benzopurpurine Self-Assembly at the Calcite–Water Interface. *The Journal of Physical Chemistry C* **2017**, *121*, 24144–24151.

(24) Silvestri, A.; Budi, A.; Ataman, E.; Olsson, M. H. M.; Andersson, M. P.; Stipp, S. L. S.; Gale, J. D.; Raiteri, P. A Quantum Mechanically Derived Force Field To Predict CO_2 Adsorption on Calcite {10.4} in an Aqueous Environment. *J. Phys. Chem. C* **2017**, *121*, 24025–24035.

(25) da Rocha, S. R. P.; Johnston, K. P.; Westacott, R. E.; Rossky, P. J. Molecular Structure of the Water–Supercritical CO_2 Interface. *J. Phys. Chem. B* **2001**, *105*, 12092–12104.

(26) Kvamme, B.; Kuznetsova, T.; Hebach, A.; Oberhof, A.; Lunde, E. Measurements and Modelling of Interfacial Tension for Water+Carbon Dioxide Systems at Elevated Pressures. *Comput. Mater. Sci.* **2007**, *38*, 506–513.

(27) Iglauer, S.; Mathew, M.; Bresme, F. Molecular Dynamics Computations of Brine–CO_2 Interfacial Tensions and Brine–CO_2–Quartz Contact Angles and Their Effects on Structural and Residual Trapping Mechanisms in Carbon Geosequestration. *J. Colloid Interface Sci.* **2012**, *386*, 405–414.

(28) Li, X.; Ross, D. a.; Trusler, J. P. M.; Maitland, G. C.; Boek, E. S. Molecular Dynamics Simulations of CO_2 and Brine Interfacial Tension at High Temperatures and Pressures. *J. Phys. Chem. B* **2013**, *117*, 5647–5652.

(29) Liu, Y.; Lafitte, T.; Panagiotopoulos, A. Z.; Debenedetti, P. G. Simulations of Vapor-Liquid Phase Equilibrium and Interfacial Tension in the CO_2–H_2O–NaCl System. *AIChE J.* **2013**, *59*, 3514–3522.

(30) Tsuji, S.; Liang, Y.; Kunieda, M.; Takahashi, S.; Matsuoka, T. Molecular Dynamics Simulations of the CO_2-Water-silica Interfacial Systems. *Energy Procedia* **2013**, *37*, 5435–5442.

(31) Müller, E. A.; Mejía, A. Resolving Discrepancies in the Measurements of the Interfacial Tension for the CO_2 + H_2O Mixture by Computer Simulation. *J. Phys. Chem. Lett.* **2014**, *5*, 1267–1271.

(32) Javanbakht, G.; Sedghi, M.; Welch, W.; Goual, L. Molecular Dynamics Simulations of CO_2/Water/Quartz Interfacial Properties: Impact of CO_2 Dissolution in Water. *Langmuir* **2015**, *31*, 5812–5819.

(33) Zhao, L.; Ji, J.; Tao, L.; Lin, S. Ionic Effects on Supercritical CO_2–Brine Interfacial Tensions: Molecular Dynamics Simulations and a Universal Correlation with Ionic Strength, Temperature, and Pressure. *Langmuir* **2016**, *32*, 9188–9196.

(34) Ji, J.; Zhao, L.; Tao, L.; Lin, S. Molecular Gibbs Surface Excess and CO_2–Hydrate Density Determine the Strong Temperature- and Pressure-Dependent

Supercritical CO_2–Brine Interfacial Tension. *J. Phys. Chem. B* **2017**, *121*, 6200–6207.

(35) Chen, C.; Chai, Z.; Shen, W.; Li, W.; Song, Y. Wettability of Supercritical CO2–Brine–Mineral: The Effects of Ion Type and Salinity. *Energy & Fuels* **2017**, *31*, 7317–7324.

(36) Liang, Y.; Tsuji, S.; Jia, J.; Tsuji, T.; Matsuoka, T. Modeling CO_2–Water–Mineral Wettability and Mineralization for Carbon Geosequestration. *Acc. Chem. Res.* **2017**, *50*, 1530–1540.

(37) Liu, S.; Yang, X.; Qin, Y. Molecular dynamics simulation of wetting behavior at CO_2/water/solid interfaces. *Chinese Sci. Bull.* **2010**, *55*, 2252–2257.

(38) McCaughan, J.; Iglauer, S.; Bresme, F. Molecular Dynamics Simulation of Water/CO_2-Quartz Interfacial Properties: Application to Subsurface Gas Injection. *Energy Procedia* **2013**, *37*, 5387–5402.

(39) Tenney, C. M.; Cygan, R. T. Molecular Simulation of Carbon Dioxide, Brine, and Clay Mineral Interactions and Determination of Contact Angles. *Environ. Sci. Technol.* **2014**, *48*, 2035–2042.

(40) Chen, C.; Zhang, N.; Li, W.; Song, Y. Water Contact Angle Dependence with Hydroxyl Functional Groups on Silica Surfaces under CO_2 Sequestration Conditions. *Environ. Sci. Technol.* **2015**, *49*, 14680–14687.

(41) Chen, C.; Wan, J.; Li, W.; Song, Y. Water Contact Angles on Quartz Surfaces Under Supercritical CO_2 Sequestration Conditions: Experimental and Molecular Dynamics Simulation Studies. *Int. J. Greenh. Gas Control* **2015**, *42*, 655–665.

(42) Chen, C.; Dong, B.; Zhang, N.; Li, W.; Song, Y. Pressure and Temperature Dependence of Contact Angles for CO_2/Water/Silica Systems Predicted by Molecular Dynamics Simulations. *Energy & Fuels* **2016**, *30*, 5027–5034.

(43) Amirfazli, A.; Hänig, S.; Müller, A.; Neumann, A. W. Measurements of Line Tension for Solid–Liquid–Vapor Systems Using Drop Size Dependence of Contact Angles and Its Correlation with Solid-Liquid Interfacial Tension. *Langmuir* **2000**, *16*, 2024–2031.

(44) Furuta, T.; Sakai, M.; Isobe, T.; Nakajima, A. Evaporation Behavior of Microliter- and Sub-nanoliter-Scale Water Droplets on Two Different Fluoroalkylsilane Coatings. *Langmuir* **2009**, *25*, 11998–12001.

(45) Raspal, V.; Awitor, K. O.; Massard, C.; Feschet-Chassot, E.; Bokalawela, R. S. P.; Johnson, M. B. Nanoporous Surface Wetting Behavior: The Line Tension Influence. *Langmuir* **2012**, *28*, 11064–11071.

(46) Werder, T.; Walther, J. H.; Jaffe, R. L.; Halicioglu, T.; Koumoutsakos, P. On the Water–Carbon Interaction for Use in Molecular Dynamics Simulations of Graphite and Carbon Nanotubes. *J. Phys. Chem. B* **2003**, *107*, 1345–1352.

(47) Ingebrigtsen, T.; Toxvaerd, S. Contact Angles of Lennard-Jones Liquids and Droplets on Planar Surfaces. *J. Phys. Chem. C* **2007**, *111*, 8518–8523.

(48) Weijs, J. H.; Marchand, A.; Andreotti, B.; Lohse, D.; Snoeijer, J. H. Origin of line tension for a Lennard-Jones nanodroplet. *Physics of Fluids* **2011**, *23*, 022001.

(49) Scocchi, G.; Sergi, D.; D'Angelo, C.; Ortona, A. Wetting and Contact-Line Effects for Spherical and Cylindrical Droplets on Graphene Layers: A Comparative Molecular-Dynamics Investigation. *Phys. Rev. E* **2011**, *84*, 061602.

(50) Becker, S.; Urbassek, H. M.; Horsch, M.; Hasse, H. Contact Angle of Sessile Drops in Lennard-Jones Systems. *Langmuir* **2014**, *30*, 13606–13614.

(51) Toshev, B. V.; Platikanov, D.; Scheludko, A. Line tension in three-phase equilibrium systems. *Langmuir* **1988**, *4*, 489–499.

(52) Widom, B. Line Tension and the Shape of a Sessile Drop. *J. Phys. Chem.* **1995**, *99*, 2803–2806.

(53) Amirfazli, A.; Neumann, A. Status of the Three-Phase Line Tension: A Review. *Adv. Colloid Interface Sci.* **2004**, *110*, 121 – 141.

(54) Méndez-Vilas, A.; Jódar-Reyes, A. B.; González-Martín, M. L. Ultrasmall Liquid Droplets on Solid Surfaces: Production, Imaging, and Relevance for Current Wetting Research. *Small 5*, 1366–1390.

(55) Hamm, L. M.; Bourg, I. C.; Wallace, A. F.; Rotenberg, B. Molecular Simulation of CO_2– and CO_3–Brine–Mineral Systems. *Reviews in Mineralogy and Geochemistry* **2013**, *77*, 189–228.

(56) Gale, J. D.; Raiteri, P.; van Duin, A. C. T. A Reactive Force Field for Aqueous-Calcium Carbonate Systems. *Phys. Chem. Chem. Phys.* **2011**, *13*, 16666–16679.

(57) Plimpton, S. Fast Parallel Algorithms for Short–Range Molecular Dynamics. *J. Comp. Phys.* **1995**, *117*, 1–19.

(58) Raiteri, P.; Demichelis, R.; Gale, J. D. Thermodynamically Consistent Force Field for Molecular Dynamics Simulations of Alkaline-Earth Carbonates and Their Aqueous Speciation. *J. Phys. Chem. C* **2015**, *119*, 24447–24458.

(59) Wu, Y.; Tepper, H. L.; Voth, G. A. Flexible Simple Point-Charge Water Model with Improved Liquid-State Properties. *J. Chem. Phys.* **2006**, *124*, 024503.

(60) Lu, C.-y.; Perez, D.; Hickmott, D. D.; Voter, A. F. Insights into Microscopic Diffusion Processes at a Solid/Fluid Interface under Supercritical Conditions: A Study of the Aqueous Calcite ($10\bar{1}4$) Surface. *J. Phys. Chem. C* **2012**, *116*, 25934–25942.

(61) Yuet, P. K.; Blankschtein, D. Molecular Dynamics Simulation Study of Water Surfaces: Comparison of Flexible Water Models. *The Journal of Physical Chemistry B* **2010**, *114*, 13786–13795.

(62) Harris, J. G.; Yung, K. H. Carbon Dioxide's Liquid-Vapor Coexistence Curve And Critical Properties as Predicted by a Simple Molecular Model. *J. Phys. Chem.* **1995**, *99*, 12021–12024.

(63) Cygan, R. T.; Romanov, V. N.; Myshakin, E. M. Molecular Simulation of Carbon Dioxide Capture by Montmorillonite Using an Accurate and Flexible Force Field. *J. Phys. Chem. C* **2012**, *116*, 13079–13091.

(64) López-Lemus, J.; Chapela, G. A.; Alejandre, J. Effect of Flexibility on Surface Tension and Coexisting Densities of Water. *The Journal of Chemical Physics* **2008**, *128*, 174703.

(65) Mei, J.; Davenport, J. W.; Fernando, G. W. Analytic Embedded-Atom Potentials for fcc Metals: Application to Liquid and Solid Copper. *Phys. Rev. B* **1991**, *43*, 4653–4658.

(66) Hockney, R. W.; Eastwood, J. W. *Computer Simulation Using Particles*; McGraw-Hill: New York, 1981.

(67) Parrinello, M.; Rahman, A. Polymorphic Transitions in Single Crystals: A New Molecular Dynamics Method. *J. Appl. Phys.* **1981**, *52*, 7182–7190.

(68) Martyna, G. J.; Klein, M. L.; Tuckerman, M. Nosé-Hoover chains: The canonical ensemble via continuous dynamics. *J. Chem. Phys.* **1992**, *97*, 2635–2643.

(69) Matsumoto, M.; Kataoka, Y. Study on Liquid–Vapor Interface of Water. I. Simulational Results of Thermodynamic Properties and Orientational Structure. *J. Chem. Phys.* **1988**, *88*, 3233–3245.

(70) de Ruijter, M. J.; Blake, T. D.; De Coninck, J. Dynamic Wetting Studied by Molecular Modeling Simulations of Droplet Spreading. *Langmuir* **1999**, *15*, 7836–7847.

(71) IAPWS Revised Release on Surface Tension of Ordinary Water Substance, June 2014. <http://www.iapws.org/relguide/Surf-H2O-2014.pdf>.

(72) Silvestri, A.; Stipp, S. L. S.; Andersson, M. P. Predicting CO_2–H_2O Interfacial Tension Using COSMO-RS. *J. Chem. Theory Comput.* **2017**, *13*, 804–810.

(73) Stipp, S. Toward a Conceptual Model of the Calcite Surface: Hydration, Hydrolysis, and Surface Potential. *Geochim. Cosmochim. Acta* **1999**, *63*, 3121–3131.

(74) Bohr, J.; Wogelius, R.; Morris, P.; Stipp, S. Thickness and Structure of the Water Film Deposited from Vapour on Calcite Surfaces. *Geochim. Cosmochim. Acta* **2010**, *74*, 5985–5999.

(75) Keller, K. S.; Olsson, M. H. M.; Yang, M.; Stipp, S. L. S. Adsorption of Ethanol and Water on Calcite: Dependence on Surface Geometry and Effect on Surface Behavior. *Langmuir* **2015**, *31*, 3847–3853.

Graphical TOC Entry